Mathematical Biosciences and Engineering

MBE, 17(5): 5099–5119.
DOI: 10.3934/mbe.2020275
Received: 16 June 2020
Accepted: 17 July 2020
Published: 27 July 2020

http://www.aimspress.com/journal/MBE

Research article

Research on land use classification of hyperspectral images based on multiscale superpixels

Hua Wang[1,*] Weiwei Li[1] Wei Huang[1], Jiqiang Niu[2,3] and Ke Nie[4]

[1] School of Computer and Communication Engineering, Zhengzhou University of Light Industry, Zhengzhou 450002, China
[2] School of Geographical Sciences, Xinyang Normal University, Xinyang 464000, China
[3] Key Laboratory for Synergistic Prevention of Water and Soil Environmental Pollution, Xinyang Normal University, Xinyang 464000, China
[4] Key Laboratory of Urban Land Resources Monitoring and Simulation, Ministry of Natural Resources, Shenzhen 518034, China

* **Correspondence:** Email: 2013016@zzuli.edu.cn; Tel: 8618137810605.

Abstract: With the rapid development of remote sensing technology, research on land use classification methods based on hyperspectral remote sensing images has attracted widespread attention. Existing land-use classification studies mostly use the average filtering method at a single scale for spectral image processing. These methods cannot accurately filter the window range, which leads to the neglect of image detail information, and the single kernel matrix cannot characterize multifeature information, resulting in reduced classification accuracy. Therefore, this study intended to use a superpixel segmentation method to perform multiscale superpixel segmentation on the first principal component of a hyperspectral image at multiple scales. By combining the weighted multiscale spatial-spectral kernel and the original spatial-spectral kernel to form a synthetic kernel for land use classification, the hyperspectral image of the National Mall in Washington DC was used as experimental data to test and analyze this method. The experimental results showed that the classification accuracy of this method on the experimental test set was 98.53%, which is compared with the classification results obtained by the single-scale spatial spectral synthetic nuclear method, the original spatial spectral synthetic nuclear method and the wavelength segmented synthetic nuclear method, the effective classification accuracy with this method was increased by 7.56%. The results prove that this method can effectively solve the problems of the lack of adaptability of the image spectrum and the lack of comprehensive spectral information and can significantly improve the accuracy of land use classification.

Keywords: multiscale; superpixel; land use classification; synthetic kernel SVM; hyperspectral

1. Introduction

Land is the foundation of human survival. Land use classification helps natural resource supervision departments remain up-to-date on the current situation of land use [1,2] and scientifically carry out land spatial planning and management. Because of their high timeliness, remote sensing images have been used as the main data source for collecting and updating land use information. Among them, hyperspectral remote sensing images can significantly improve the differentiation and recognition of ground features due to their rich image spectral information and are favored by researchers [3–5].

At present, the land use classification methods that have been developed based on remote sensing images are the maximum likelihood method [6], decision tree method [7,8], support vector machines (SVM) [9,10], artificial neural networks [11], unsupervised feature learning method [12], deep learning models [13,14] and other artificial intelligence and machine learning methods. These methods have greatly improving the efficiency and accuracy of land use classification, among which the existing land use classification method based on SVM algorithm Including multi-feature method, superpixel method and synthetic kernel method, etc.. The land use classification method that combines superpixel and synthetic kernel at multiple scales needs to be studied for its feasibility and efficiency. Compared with general remote sensing images, hyperspectral remote sensing data not only provide image features but also provide a large number of subtle spectral features [15,16], making traditional pixel-by-pixel methods extremely susceptible to noise; during the extraction of image features, the importance of clustering similar features is often ignored, which reduces the classification accuracy [17]. Image segmentation is part of the research classification method, and there are many methods for image segmentation [18–20], among them superpixels can divide pixels with similar spatial positions in the image and similar characteristics of color, brightness, texture, etc. into small areas, which can abstract pixel-level images into high-dimensional data at the regional level [21]. It is a widely used image segmentation method. For example, Song et al. used the SLIC algorithm for superpixel segmentation of damaged building images [22]. B. Amin et al. used the SLIC algorithm to perform superpixel segmentation of images acquired by the synthetic-aperture radar (SAR) sensor [23]. Yuan et al. used the SLIC algorithm to perform superpixel segmentation of near-infrared starry sky images [24]. The superpixel method can be used to cluster adjacent pixels with similar textures and spectral characteristics in hyperspectral remote sensing images [25]. Superpixels combined with the spatial-spectral kernel (SSK) method can effectively extract the spatial similarity features of a sample hidden in the high-dimensional kernel feature space. For example, Chen et al. used the superpixel spatial-spectral kernel method to classify hyperspectral images, resulting in a classification accuracy that was superior to the current most advanced classification methods [26]. Liu et al. completed small target detection under a complex background based on a superpixel image model, which greatly improved the accuracy of target detection [27]. Chaibou MS et al. developed a new segmentation algorithm based on superpixel context features to obtain superpixel-segmented images with better effects [28]. Song et al. combined superpixels with supermetric contour maps to form superpixel segmentation algorithms with low parameter dependence and high segmentation accuracy [29]. Hou et al., based on superpixel multifeature fusion,

created a superpixel segmentation method with a faster segmentation time than the other compared algorithms [30]. The abovementioned superpixel segmentation methods are widely used in medical image processing, military target detection and other fields, and the research results show that improved methods based on superpixels can effectively improve the accuracy of target classification. However, land use classification based on superpixel segmentation still has the following defects: (1) Superpixels generally perform image segmentation under an initial number of superpixels. If the initial value of superpixels is too small, key discriminating information may be lost. If the initial value is too large, it may contain too much interference information, so the optimal number of initial superpixels is not easy to determine [31]. (2) Single-scale feature extraction and single-kernel feature classification have greater difficulty in extracting finer image information. A more reasonable method should extract as much comprehensive discriminatory information as possible while reducing the interference information [32].

Based on the above research, in order to effectively improve the accuracy of land use classification based on hyperspectral remote sensing images, this paper proposes a land-use classification method that couples multi-scale superpixel segmentation and synthesis kernel (Multi-scale spatial spectrum synthesis kernel, Ms-SSSK). This method considers image segmentation at multiple scales and merges the segmented images at all scales, it is helpful to extract more comprehensive image feature information [33,34]. This method uses principal component analysis to obtain the main band information of the original hyperspectral data to form the first principal component, and uses the superpixel segmentation method to extract the spatial-spectral kernel matrix of the principal component image at multiple scales. The original spectral kernel of the image is combined with the weight to form a multiscale spatial-spectral synthesis kernel matrix. Finally, the support vector machine algorithm is trained on the matrix and used to predict land use classifications. In this study, the HYDICE for the National Mall in Washington DC [35] was used as the experimental data to implement and test the method on the MATLAB platform, after the classification accuracy of the ideal test set is obtained, the model is applied to Botswana and Pavia Centre hyperspectral data [36] to comprehensively evaluate the model. And the land use classification results obtained with this method were compared with the single-scale spatial-spectral synthesis kernel (Ss-SSSK) method, the original spatial-spectral synthesis kernel (O-SSSK) method and the wavelength segmented synthetic kernel (WSSK) method to verify the effectiveness and feasibility of the improved method.

2. Materials and methods

2.1. Materials selection and processing

The hyperspectral data set used in this article is Washington DC Mall. Because this article needs to determine the classification status of the features in this area, the DC hyperspectral remote sensing image is used as the research object to achieve the classification goal. After removing the opaque band, the number of remaining bands is 191, and the pixel size is 1280 × 307 × 191. In this study, the image data below 591 lines (690 × 307 × 191) were used as the research object, and according to the actual situation on the ground, the research area was divided into 7 categories: Residential, highway, street, grass, woodland, water and shadow. Each band contains 211830 pixels, of which 5471 pixels have a certain classification label, so as a sample set for the construction of experimental models, in this

project, the sample set is used to build classification model, and use the model to achieve the land use classification goal of the research object. The number of training sets and test sets of the 7 categories in the article is shown in Table 1 below.

Table 1. Number of sample categories and sample sets.

Category	Number of training sets	Number of test sets
residential	500	3365
highway	60	356
street	50	89
grass	60	358
woodland	60	345
water	60	389
shadow	30	39

The hyperspectral image used in this study had 191 bands, and each pixel contained a large amount of spectral information. In addition, there was a close spatial and spectral relationship between the adjacent bands. If the spectral information of all bands was used for the experiment of image spatial-spectral kernel formation, the experimental time would have been prolonged, and the experiment would have been labor intensive due to the large data dimensions [37]. Therefore, to form the spatial-spectral nucleus quickly and efficiently, it was necessary to reduce the dimensionality of the hyperspectral image. The purpose was to select the main components that contained most of the spatial-spectral characteristics of the hyperspectral image in many bands, and then to use the principal components for experiments, which could greatly improve the classification efficiency.

At the same time, this article uses the hyperspectral data sets Botswana and Pavia Centre to comprehensively evaluate the model, the purpose is to verify the high applicability of the classification model proposed in the article. Hyperspectral data Botswana is obtained by NASA EO-1 satellite. After removing the interference band, the number of remaining bands is 145. The pixel size of the image is 1476 × 256 × 145. The image size used in this article is 751 × 256 × 145, which is hyperspectral Part of the data Botswana. According to the actual situation on the ground, this study is divided into 14 categories such as water, exposed soil, floodplain grasses1, each band of the image contains 192256 pixels, and the number of pixels of the known classification label is 2909. Among them, there are 666 training sets and 2243 test sets. The size of the hyperspectral data Pavia Centre is 1096 × 715 × 102, and the image size used in this article is 481 × 291 × 102, which is part of the hyperspectral data Pavia Centre. According to the actual situation on the ground, this study is divided into 9 categories including Water, Trees, Meadows, etc. Each band of the image contains 139971 pixels, and the number of pixels of the known classification label is 15489, including 2310 training sets and 13179 test sets.

In general, the algorithms used to reduce data dimensionality include linear discriminant analysis (LDA), principal component analysis (PCA), and locally linear embedding (LLE). The most commonly used is the principal component analysis algorithm. In this study, we used principal component analysis for the same pixel to find a band that represented most of the original image and to perform image segmentation. Principal component analysis (PCA) is a widely used dimensionality reduction method [38,39]. The dimensionality reduction steps were as follows: (1) The original hyperspectral image $a * b * c$ was inputted and the original matrix was processed into a

two-dimensional matrix of $m*n\left(m=a\times b\right)$. (2) The mean (μ) of the $m*n$ matrix and the covariance matrix (C) $n\times n$ was identified, and the eigenvalue (λ) and eigenvector (E) of C were calculated. (3) The feature values were arranged in order from large to small. The larger the feature value was, the more important the feature. If only the first p features were extracted, the first p column vectors in E were selected to construct the pattern matrix Ep. (4) The original image was decentralized to form matrix A, and finally, the matrix was formed after dimensionality reduction by calculating $\left[E_p^T\times A^T\right]^T$. In this study, the first principal component was obtained by calling the PCA function in MATLAB to implement data dimensionality reduction, and the contribution rate was 81.7%. The process is shown in Figure 1.

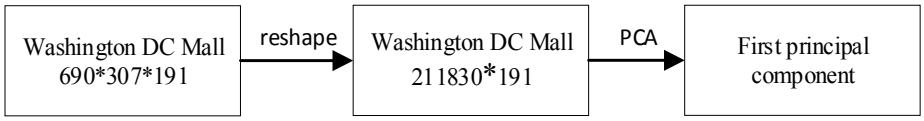

Figure 1. Principal component extraction flowchart.

After the PCA algorithm was used to extract the first principal component of the hyperspectral image, the first principal component needed to undergo superpixel segmentation to ensure that the adjacent pixels with the same or similar spectral characteristics belonged to the same category label. After the superpixels were segmented, the calculation operation was performed according to the superpixel area blocks, avoiding the tedious process of pixel-by-pixel calculation.

At present, the commonly used algorithms for superpixel segmentation include a superpixel segmentation algorithm based on entropy rate (ERS), superpixel segmentation algorithm based on the gradient descent method (SLIC), graph-based superpixel segmentation algorithm (graph-based), etc.. ERS calculates the function value of the edge between each pixel vertex and its neighbor by defining the objective function. The larger the function value, the higher the similarity of the two pixels and the greater the possibility of belonging to the same category. Delete the edge with the largest function value to make the two pixels. It belongs to a superpixel, and all vertices of the pixels are calculated in sequence until the number of superpixels is equal to the set superpixel value. Segmenting the image by the ERS algorithm can retain the image edge information to the greatest extent, and then generate a superior superpixel image, so its good segmentation the effect is favored by the majority of researchers [40,41]. The classification information to distinguish grassland, woodland and other features in the study area has higher requirements for edge discrimination. Therefore, this paper uses the ERS segmentation method [42] to perform superpixel segmentation on the extracted principal components at multiple scales to ensure that the features that are more difficult to obtain in one scale are easily extracted in other scales [43]. The value of each scale needs to satisfy $M = 2^{n-1}$ [44], where n is the number of scales, the number of superpixels $N = M * k$, and k is the number of basic superpixels. Following existing research [45], this paper selected 4 scales for image processing, the initial pixel number k was set to 400, and the superpixel segmented images at each scale are shown in Figure 2.

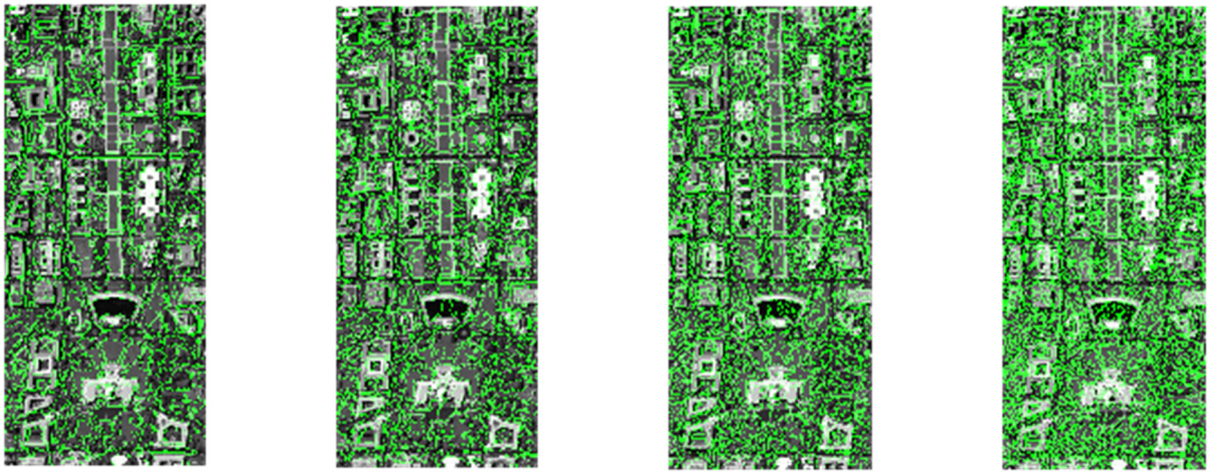

(a) N = 400 (b) N = 800 (c) N = 1600 (d) N = 3200

Figure 2. Superpixel segmentation image.

2.2. Methods

The classification algorithm used in this study was a support vector machine. Support vector machines (SVMs) are commonly used machine learning algorithms that can effectively solve classification problems [46–50]. It shows good classification results for the problems of high dimensionality and low sample size. The method is most commonly used in linear classification problems; to address linearly separable problems, it is necessary to complete the mapping from low-dimensional space to high-dimensional space through the kernel function and then to conduct classification research [51]. If the sample set $S = \{(x_1, y_1), (x_2, y_2), \cdots, (x_n, y_n)\}$, then $x_i \in R^N$, $y_i \in \{1, -1\}$, and $i = 1, 2, 3, \cdots, n$, where x_i represents the input sample and y_i represents the corresponding class label of the sample. For a linearly separable classification problem, Eq (1) can be used to solve the quadratic programming problem. The SVM finds the optimal classification hyperplane through this method to achieve the goal of sample classification.

$$\min\left\{\frac{\|\omega\|^2}{2} + C*\left(\sum_{i=1}^{n}\xi_i\right)\right\} \tag{1}$$

$$s.t.y_i\left(\omega x_i + b\right) - 1 \geq 0, i = 1, 2, \cdots, n \tag{2}$$

where the parameter ω represents the normal vector of the hyperplane, b is the linear classifier parameter, C is the penalty factor that can affect the generalization and classification performance of the classifier, and the parameter ξ_i affects the acceptable error range. The optimal classification is obtained from the above formula. The hyperplane is as follows:

$$f\left(x\right) = \left\{\text{sgn}[\sum_{i=1}^{n} y_i a_i^*\left(x, x_i\right) + b^*]\right\} \tag{3}$$

In Eq (3), a^* is the Lagrange multiplier, and b^* is the threshold. For the linear inseparable problem, the optimal classification hyperplane is as follows:

$$f(x)=\left\{\operatorname{sgn}[\sum_{i=1}^{n} y_i a_i^* \mathrm{K}(x,x_i)+b^*]\right\} \tag{4}$$

In Eq (4), $K\ (x,\ x_i)$ is a kernel function that is defined as follows:

$$K(x,y)=\langle\phi(x),\phi(y)\rangle \tag{5}$$

where ϕ is the mapping. Commonly used kernel functions are the sigmoid kernel function, Gaussian (radial basis function, RBF) kernel function and linear kernel function. For large and small samples, the RBF kernel function can have good performance, and relatively few parameters are involved [52]. Therefore, this study chose the RBF kernel function for research, and it is expressed as follows.

$$K(x_i,x_j)=\exp\left(-\left\|x_i-x_j\right\|/2\delta^2\right) \tag{6}$$

where δ is the width parameter, and the selection of this value will have a greater impact on the classification accuracy. Based on two effective kernels K_1 and K_2, a new effective kernel can be generated by the following formula:

$$K(x_i,x_j)=K_1(x_i,x_j)+K_2(x_i,x_j) \tag{7}$$

$$K(x_i,x_j)=K_1(x_i,x_j)\bullet K_2(x_i,x_j) \tag{8}$$

$$K(x_i,x_j)=\mu K_1(x_i,x_j);\mu>0 \tag{9}$$

The newly constructed kernel function $K(x_i,x_j)$ is a combination of K_1 and K_2, and K_1 and K_2 can be applied to hyperspectral remote sensing image data from different sources and phases [53]. In this study, the spatial-spectral features at different scales were combined using Eq (7) to form a new spatial-spectral kernel, and the spatial-spectral kernel was combined with the original spectral kernel to form a synthetic kernel by Eq (9) in the form of a weighted value.

The hyperspectral remote sensing image used in this study is subjected to PCA to extract the principal components, and the first principal component containing most of the image features is obtained. And then the first principal component is superpixel segmented at multiple scales and the superpixel features are defined it's the average of the spectral characteristics of all pixels in the superpixel. The linear inner product is calculated by the RBF kernel function of the eigenvalues of two adjacent superpixels. The calculation result represents the similarity between the two superpixels, so that the original space samples are mapped to the kernel space to form a kernel matrix. Suppose that a pixel in the experiment is $S_i=\{x_{i1},x_{i2},x_{i3},\cdots,x_{ik}\}$, the superpixel, where k is the total number of pixels in the superpixel, $x_{i1},x_{i2},x_{i3},\cdots,x_{ik}$ is the k pixels included in the superpixel, a superpixel is a collection of multiple pixels, and its spectral mean can be calculated by Eq (10).

$$S_i^{mean} = 1/k * \left(\sum_{i=1}^{k} X_{ik} \right) \tag{10}$$

In a superpixel, all pixels belong to the same category, so while S_i^{mean} represents the spectral average feature of the superpixels, it can also represent the spatial-spectral characteristics of all pixels in the superpixel. Any superpixel has its own unique characteristics, and the similarity between two different superpixels S_i and S_j was calculated by the following formula:

$$\left\langle \phi(S_i), \phi(S_j) \right\rangle = K(S_i, S_j) = K\left(S_i^{mean}, S_j^{mean}\right) \tag{11}$$

During the experiment, the sample set is divided into a training set and a test set. The training set is used to build a classification model, and the test set is used to verify the performance of the model to ensure that the classification results in the global area of the Washington DC shopping mall are close to the real feature classification. The result calculated by Eq (11) is the spatial spectral kernel matrix, traversing the superpixel position of each pixel in the training set and extracting the training kernel matrix, the training kernel matrix of n training samples is $n \times n$. And then find the superpixel position of each pixel in the test sample in the kernel space, and find the similarity with the superpixels where all training samples are located to form the test kernel matrix. The kernel matrix obtained by different image scales is different, so combined with the image feature kernel matrix obtained at multiple scales, more subtle image features can be considered. Multiple training kernel matrices and test kernel matrices at different scales respectively pass the Eq (12) calculate a new kernel matrix, where M is the number of scales.

$$K(X_i, X_j) = 1/M * \left(\sum_{s=1}^{M} K_s(X_i, X_j) \right) \tag{12}$$

The Ms-SSSK method includes the spatial spectral kernel matrix and the original spectral kernel matrix. The spatial spectral kernel matrix of the training set and the test set can be obtained from Eq (12). The original spectral kernel matrix is derived from the original spectral information of each pixel in the sample set obtain. Each pixel of the original hyperspectral image contains rich spectral information, so the spectral mean can be used as a reliable original spectral feature to obtain the original spectral kernel matrix. If $s = (s_1, s_2, s_3, \cdots, s_n)$ is the spectral value of any pixel in n bands, then the original spectral mean of the pixel is $s^{mean} = \frac{1}{n} \sum_{i=1}^{n} s_i$. By taking s^{mean} as the original spectral feature of a pixel, the arbitrary pixels X_i and X_j in the sample set can be expressed by $K\left(S_i^{mean}, S_j^{mean}\right)$.

$$K = \mu K_{pp} + (1 - \mu) K_{yp} \tag{13}$$

The extraction of spatial spectral information is conducive to the establishment of the spatial relationship between the pixels, and the extraction of original spectral information pays more attention to the spectral differences between the objects to distinguish different objects. Extract the original

spectral kernel matrix of the training set and the test set from the original spectral kernel matrix, and combine the spatial spectral kernel matrix of the training set and the test set with the original spectral kernel matrix by Eq (13). The combination method is the weight assignment, adjust the proportion of the spatial spectral kernel matrix and the original spectral kernel matrix according to the weights, to get the final training synthetic kernel matrix and test synthetic kernel matrix, where μ is the balance parameter, K_{pp} is the spatial-spectral kernel matrix, and K_{yp} is the original spectral kernel matrix. which is ultimately used to construct a classification model of Ms-SSSK, is calculated by Eq (14).

$$\begin{aligned} K_{Ms-SSSK}\left(X_i, X_j\right) &= \mu K_{pp}\left(X_i, X_j\right) + (1-\mu) K_{yp}\left(X_i, X_j\right) \\ &= \mu\left(\frac{1}{M}\sum_{s=1}^{M} K_s\left(X_i, X_j\right)\right) + (1-\mu)\left(\frac{1}{n}\sum_{i=1}^{n} S_i\right) \end{aligned} \tag{14}$$

The training kernel matrix and the testing kernel matrix are calculated by Eq (14). And the SVM software package libsvm is used to construct the classification model and predict the classification result of the test sample set, which is used to verify the classification performance of this method and obtain the classification of the samples in the whole area is obtained. And the status of land use classification in this area is observed. In this paper, the multi-scale spatial spectral kernel and the original spectral kernel are combined to form Ms-SSSK, which is applied to land use classification. This method takes into account the original spectral characteristics while considering the image spatial spectral relationship, and considers more comprehensive and subtle image characteristics. The overall research process is shown in Figure 3.

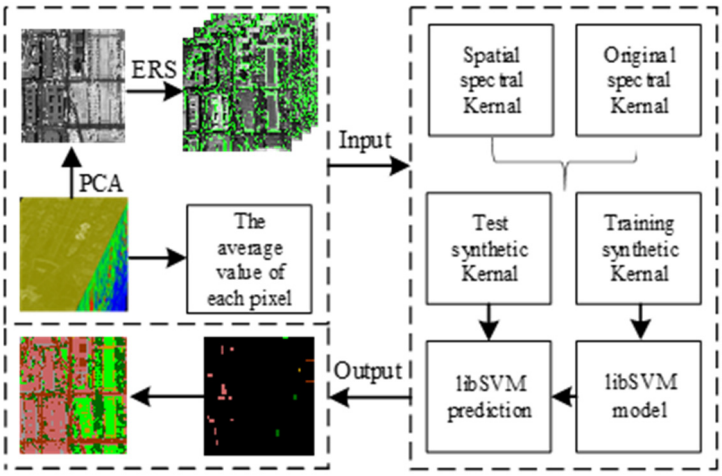

Figure 3. Overall flowchart.

3. Results

3.1. Experimental program

In this paper, based on the original Ms-SSSK method, three sets of control experiments are set up, namely Ss-SSSK, O-SSSK and MSSK. The calculation method of each group of experiments

was as follows:

1) Ss-SSSK method

The Ss-SSSK consists of a single-scale superpixel spatial-spectral kernel and the original spectral kernel, where the single-scale superpixel spatial-spectral kernel was obtained as shown in Figure 4.

The spectral average information of all bands of each pixel of the original hyperspectral image were obtained, and the original spectral kernel matrix was obtained through the RBF kernel function. The single-scale superpixel spatial-spectral kernel matrix and the original spectral kernel matrix were combined to form the Ss-SSSK for land use classification.

2) O-SSSK method

O-SSSK consists of the original spatial-spectral kernel and the original spectral kernel. The original spatial-spectral kernel was obtained as shown in Figure 5.

The first principal component of the hyperspectral image was obtained, then a 5 × 5 window was used to extract the spectral mean of the principal component image, and the RBF kernel function was used to obtain the original spatial-spectral kernel matrix. The original spatial-spectral kernel matrix and the original spectral kernel matrix were combined by weight to form the O-SSSK for land use classification.

3) MSSK method

MSSK is realized by a spectral synthesis kernel formed by combining wavelength segments, and the synthesis kernel is obtained as shown in Figure 6.

The hyperspectral image contains multiple bands, divide the first half of the band into a group, and then divide the second half of the band into a group, extract the feature information of each pixel according to the grouping situation, and obtain the kernel matrix of each group through the kernel function. Then use the weights to combine the two kernel matrices to form MSSK for land use classification.

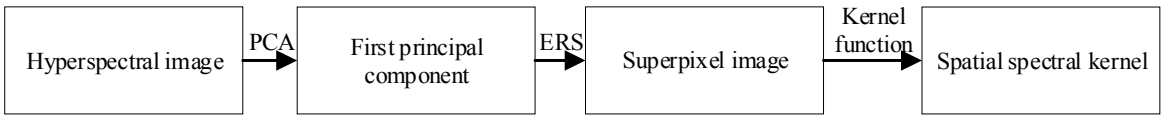

Figure 4. Single-scale superpixel spatial spectrum kernel acquisition flowchart.

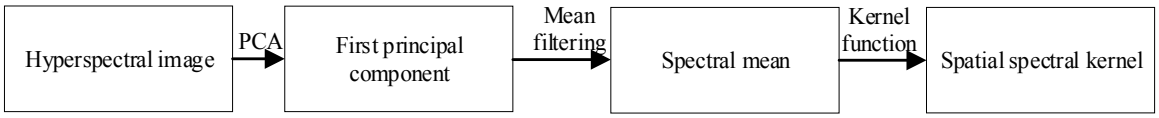

Figure 5. Original spatial-spectral kernel acquisition flowchart.

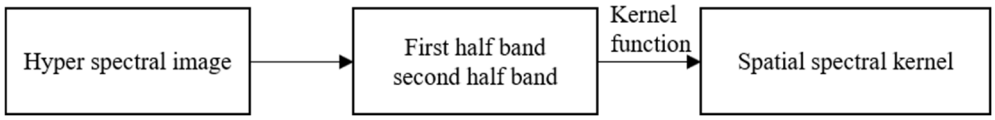

Figure 6. synthesis kernel acquisition flowchart.

3.2. Analysis of Ms-SSSK model results

In this paper, the hyperspectral image with 191 effective spectral bands was selected as the analysis object, the 5471 sample points of the known feature categories in the sample set were labeled, and 820 samples were randomly selected as the training set to construct the classification model. The remaining 4651 samples were used as test sets to verify the performance of the classification model. The RBF kernel was selected to construct the Ms-SSSK classification model and, combined with 7 cross-validation and grid searches, the optimal kernel function parameter value g was 9.196, and the optimal penalty factor c was 16.489.

When the synthetic nuclei in the Ms-SSSK method are formed, the selection of the parameter μ has a certain effect on the classification accuracy [53], so the Ms-SSSK method searches for the weight value in increments of 0.1 in the interval [0,1]. The experimental program is run 5 times under each μ value and the average classification accuracy is calculated to find the best μ value to obtain the highest average classification accuracy. For the test set, the classification accuracies under different weights μ are shown in Figure 7 below.

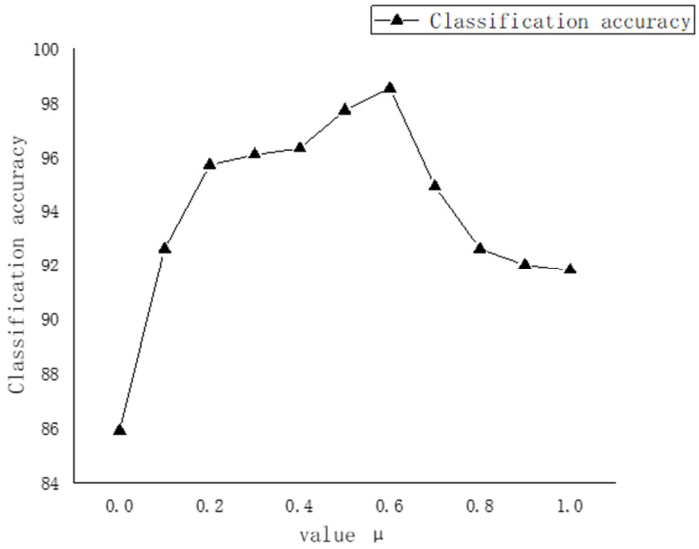

Figure 7. Classification accuracy map corresponding to the weight μ.

It can be seen from Figure 7 that the classification accuracy obtained by different weight coefficients is different. The symbol μ in the synthetic kernel is the spatial spectral kernel weight coefficient, and $(1-\mu)$ is the original spectral kernel weight coefficient. When μ is 0 or 1, it means that the final classification kernel matrix is composed of a single kernel, and the classification accuracy of the single original spectral kernel is 85.87%, which is lower than the single spatial spectral kernel classification accuracy of 91.79%. When μ is 0.1–0.6, the classification accuracy continues to rise, at this time the proportion of multi-scale spatial spectral kernel gradually increases, and the proportion of original spectral kernel gradually decreases. When μ is 0.6–0.9, the classification accuracy begins to decrease. At this time, the multi-scale spatial spectral kernel accounts for a larger proportion, and the original spectral kernel accounts for a smaller proportion.

When μ is 0.6, the classification accuracy is 98.53%. At this time, the classification accuracy is high, and the proportion of the multi-scale spatial spectral kernel is slightly higher than the original spectral kernel, it avoids the phenomenon that stars and dots are classified due to the relatively large kernel of the original spectral. When μ = 0.6, the spatial spectral synthesis kernel formed by the combination of the two kernel matrices considers more comprehensive and fine feature information, and reasonable combination of the original spectral features can obtain higher classification accuracy. The test set classification results under partial weight μ are shown in Figure 8.

During the land-use classification experiment based on the Ms-SSSK method, both the spatial-spectral kernel and the original spectral kernel used to construct the synthetic kernel played an important role, and the contribution rate of the spatial-spectral kernel was slightly higher than that of the original spectrum nucleus. All kinds of ground features have their own unique spectral characteristics, but the phenomenon of homogenous foreign objects and heterogeneous spectra occurs from time to time. In the Ms-SSSK method, when the original spectral features account for a large amount of the image, the finer spatial-spectral features do have an advantage, and it is easy to cause the overall classification accuracy to decrease. Using the weight μ to reasonably allocate the spatial and original spectral features can greatly improve the accuracy of land use classification.

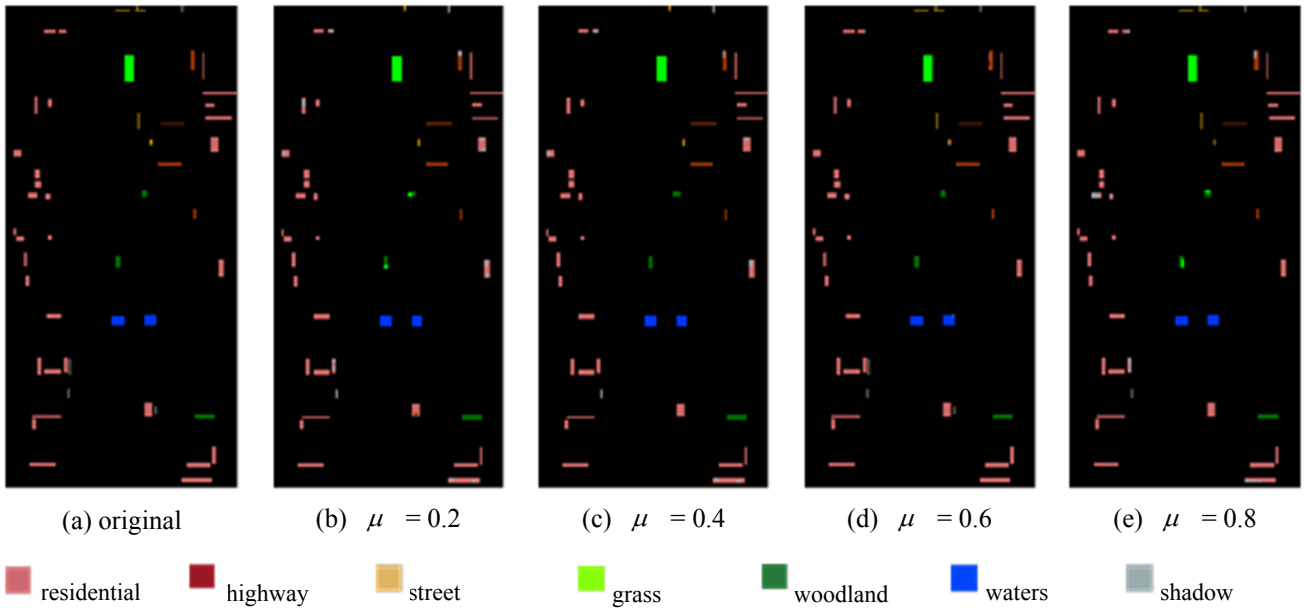

Figure 8. Classification results corresponding to some μ values.

4. Discussions

When μ was 0.6, according to the original c, g parameters and the number of training set and test set, the source programs of the classification methods Ms-SSSK, Ss-SSSK O-SSSK and MSSK were respectively run 5 times, and the average classification accuracy results on the test set are shown in Table 2.

It can be seen from the table that the classification accuracy of the Ms-SSSK method is the highest, reaching 98.53%, and the classification accuracy of the MSSK method is the lowest, 90.97%. Compared with the MSSK method, the classification accuracy of O-SSSK is improved by 0.63

percentage points; compared with the Ss-SSSK, O-SSSK, and MSSK methods, the classification accuracy of Ms-SSSK is improved by 3.2, 6.93, and 7.56 percentage points, respectively, and the four models The test set classification results are shown in Figure 9.

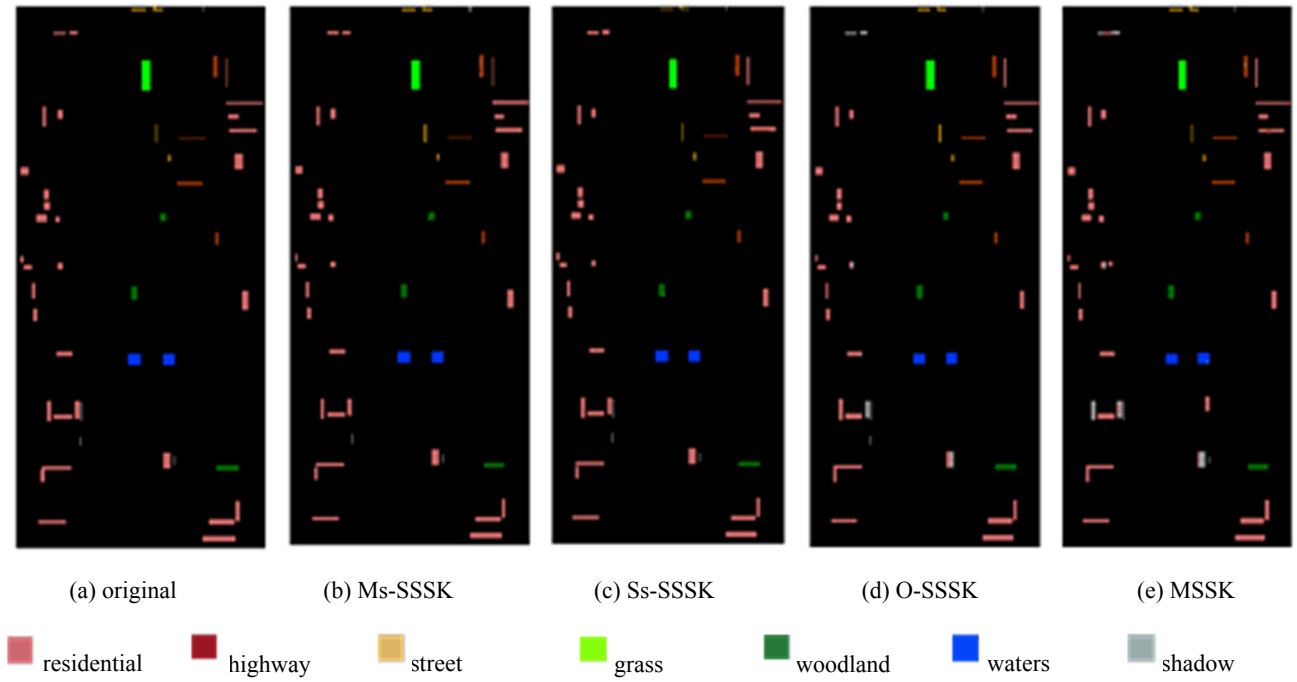

Figure 9. Classification result of the test set.

Figure 9 (a) shows the original test set. Figure 9 (b) displays the land use classification result obtained by the Ms-SSSK method. Only 68 pixels in the test set were not correctly classified, of which 28 were residential and 15 were grassland, 9 were forestland, and the remaining 16 were roads, streets, water and shadows. Figures 9 (c,d,e) shows the classification results obtained by the Ss-SSSK , O-SSSK and MSSK methods, respectively. The classification accuracy of all feature categories in the test set was obtained by three methods as shown in Table 3.

As shown in Table 3, among the four land-use classification methods, the classification accuracies of shadow, highway, and grass obtained by using the Ms-SSSK method were greatly improved. Among them, shadows increased from 87.91% of MSSK method, 87.73% of O-SSSK method, and 96.60% of Ss-SSSK method to 98.16% of Ms-SSSK method. The shadow area in the dataset was small, but the distribution was scattered. When the residential area was large, it was easy to classify residential areas, and shadow were divided into one category. The classification accuracy of grass has increased from 88.75% of MSSK method, 89.16% of O-SSSK method, and 92.12% of Ss-SSSK method to 97.35% of Ms-SSSK method. The woodland and grass in the study area were not sufficiently spatially distributed and spread throughout the area, and the two had relatively similar spectral characteristics, so grass and woodland were easily confused when they were classified. The classification accuracy of highways has increased from 87.55% of the O-SSSK method, 91.20% of the MSSK method, and 92.68% of the Ss-SSSK method to 98.32% of the Ms-SSSK method. And the road occupied a large portion of the entire area and was adjacent to pixels such as grass, woodland, and

residential pixels, so it could easily be mistakenly classified into the abovementioned types of land during classification.

Table 2. Comparison of results.

Parameter result value	Ms-SSSK	Ss-SSSK	O-SSSK	MSSK
g parameter	9.196	9.196	9.196	9.196
c parameter	16.489	16.489	16.489	16.489
μ parameter	0.6	0.6	0.6	0.8
Overall accuracy (%)	98.53	95.33	91.60	90.97
Kappa	0.9601	0.9216	0.9031	0.8790

Table 3. Classification accuracy of each category obtained by different methods (%).

category	Ms-SSSK	Ss-SSSK	O-SSSK	MSSK
residential	99.28	98.30	96.67	89.69
highway	98.32	92.68	87.55	91.20
street	98.70	96.70	91.60	92.13
grass	97.35	92.12	89.16	88.75
woodland	97.60	96.37	93.65	92.37
water	98.65	98.71	96.87	93.31
shadow	98.16	96.60	87.73	87.91

The Ss-SSSK method divided the image into superpixels at one scale and was unable to determine the optimal number of original superpixels. Compared with multiscale superpixels, it was impossible to consider finer image feature information, so it was difficult to obtain a classification effect greater than the Ms-SSSK method. The O-SSSK method used the filter window to obtain the image spatial-spectral mean information. However, the size of the optimal window was difficult to determine; if the window was too small, it as unable to contain all important information; if the window was too large, it contained interference information. Compared with the use of superpixels, it was not possible to adaptively calculate the average area, so it was difficult to obtain a classification effect greater than that of the Ss-SSSK method. The MSSK method uses wavelength segmentation to obtain image spectral information, considering that there is less spatial information, so the classification accuracy obtained is difficult to exceed the O-SSSK method, but the difference is not large.

It can be seen from the above that the Ms-SSSK model has obtained high classification accuracy in the test set of the hyperspectral data set National Mall in Washington DC. The model is applied to the hyperspectral data of Botswana and Pavia Centre, and then the experimental classification results are compared, it is beneficial to comprehensively evaluate the performance of the model. Applying the four models to the Botswana and Pavia Centre data sets, the classification results of the test set are shown in Figures 10 and 11.

As shown in Figures 10 and 11, the Ms-SSSK method proposed in this paper can obtain good classification results in the hyperspectral image datasets Botswana and Pavia Centre. Therefore, using the Ms-SSSK model for regional feature classification in the whole region can maximize the closeness to the real feature information. Applying this model to the Washington DC full-area image, the resulting land-use classification results are shown in Figures 12 and 13.

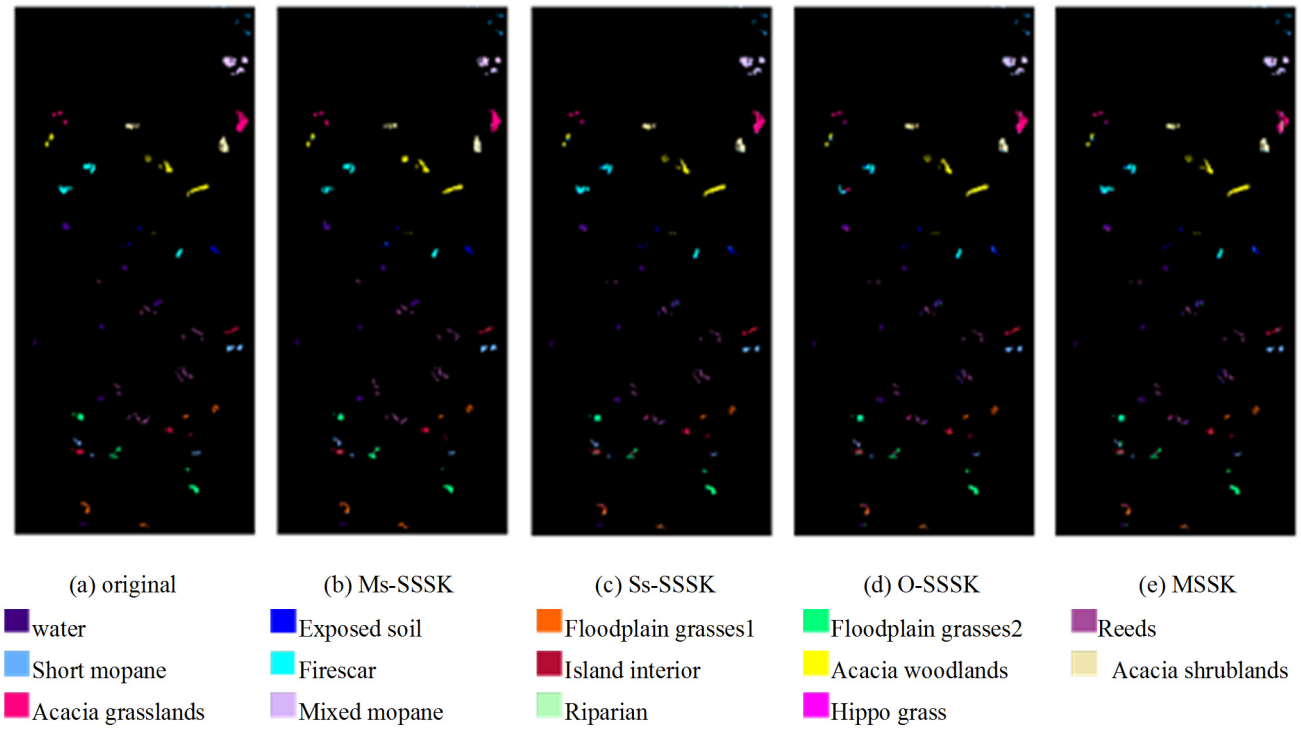

Figure 10. Classification results of hyperspectral data Botswana test set.

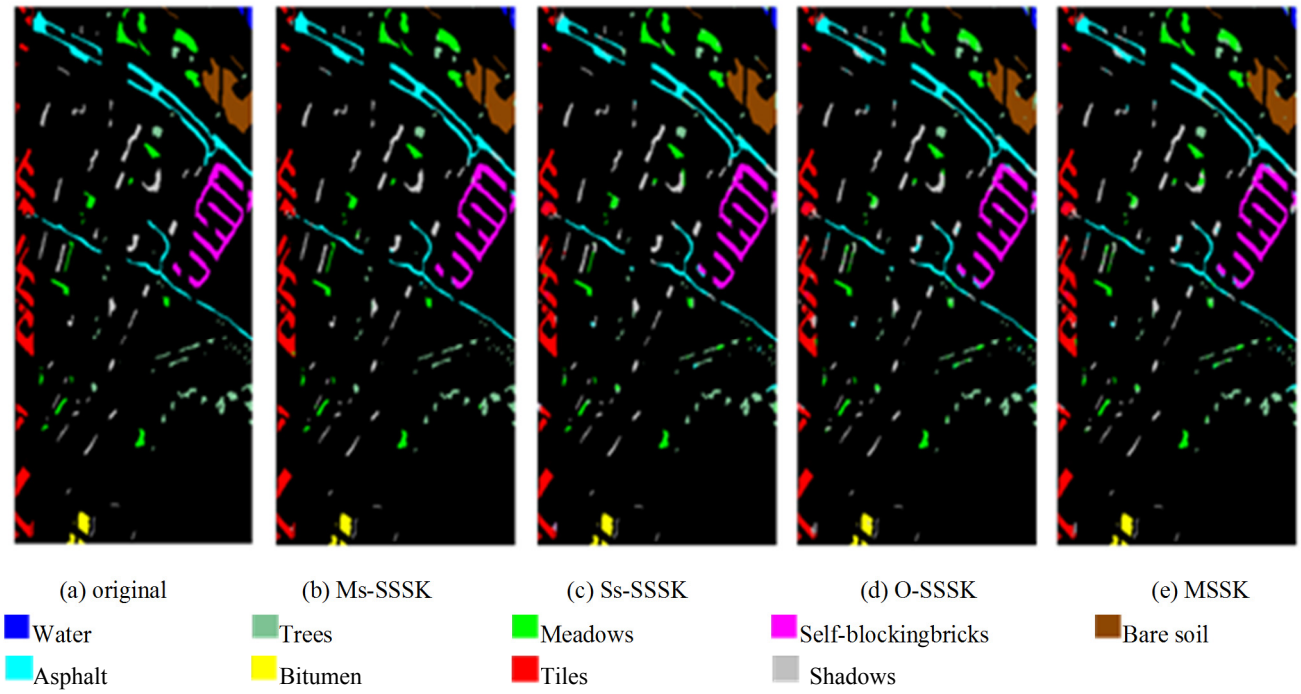

Figure 11. Classification results of hyperspectral data Pavia Centre test set.

Figure 12(a) is the image of the original research area, and two typical areas were selected for the comparison of classification details. The specific land use categories are shown in Figure 13(a). Figure 12(e) is the classification result of the MSSK method. This method is easy to confuse grass and

woodland with similar spectra, and it is easy to divide the highway in small areas into shadow, as shown in Figure 13(e). Figure 12(d) shows the classification result of the O-SSSK method. This method can roughly classify 7 kinds of features but lacks spatial details, as shown in Figure 13(d). Figure 12(c) shows the classification result of the Ss-SSSK method. The shadow details in the picture were more obvious, but the overall land use classification results had more errors, especially highway and grass, as shown in Figure 13(c). Figure 12(b) showed the classification results of the Ms-SSSK method. The image features considered by this method were more elaborate. Compared with the other three methods, the image details were distinguished more clearly (as shown in Figure 13(b)), and a higher accuracy of feature classification was obtained.

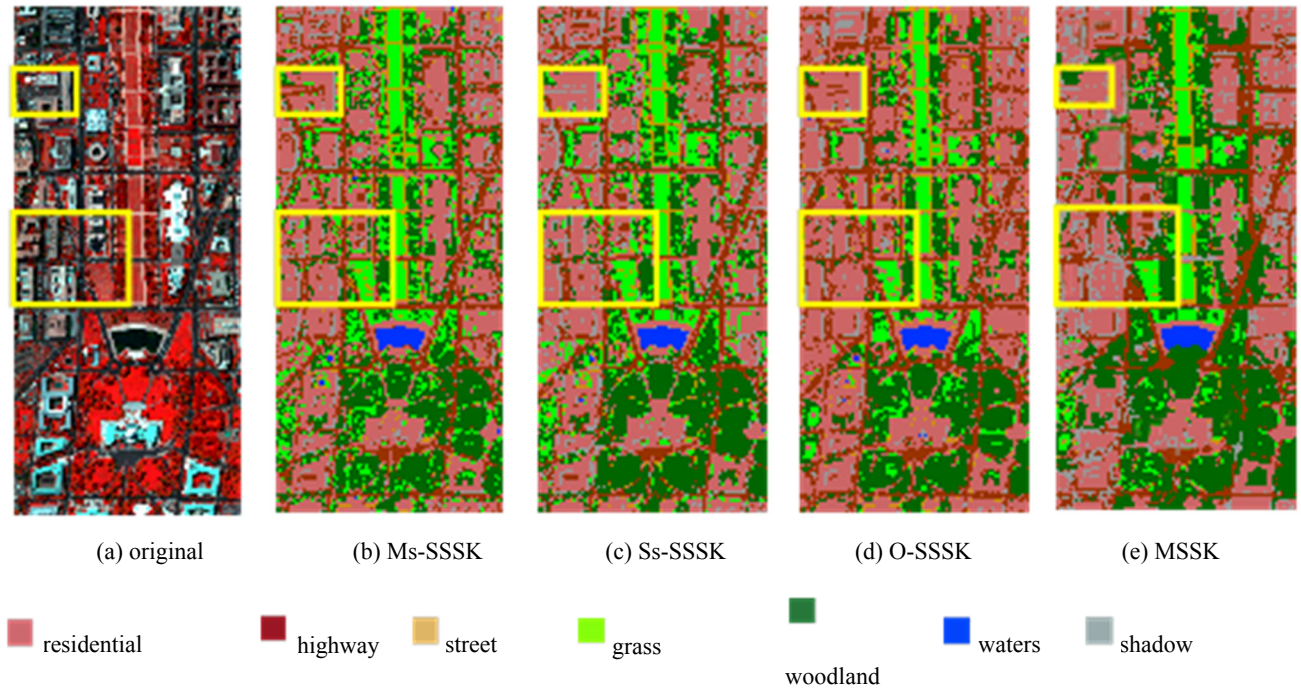

Figure 12. Overall image comparison.

This article continued to explore the classification accuracy of the above methods on sample sets of different scales. Two hundred, 400, 600, and 800 sample points were randomly selected from the sample set to train the model, and the remaining samples were used as test sets to verify the model performance. The relative errors of the models for different scale test sets are shown in the figure below. Figure 14 shows that the sample size increased from 200 to 800, and the classification error of each model continuously decreased. When the number of samples was 200, the relative error of the Ms-SSSK model classification was 10.28%, and it had the largest gaps with the other three models, with 4.68, 9.51 and 8.68% higher, respectively. As the number of samples increased, the classification accuracy gap gradually narrowed to 2.27, 4.45 and 5.36%. This result proves that the spatial-spectral synthesis kernel method of the Ms-SSSK model can learn the similar features of the samples in the kernel space and then merge the multidimensional features of the image to obtain more detailed and sufficient image information. When the training sample set is small in scale, it can still obtain an ideal land use classification accuracy.

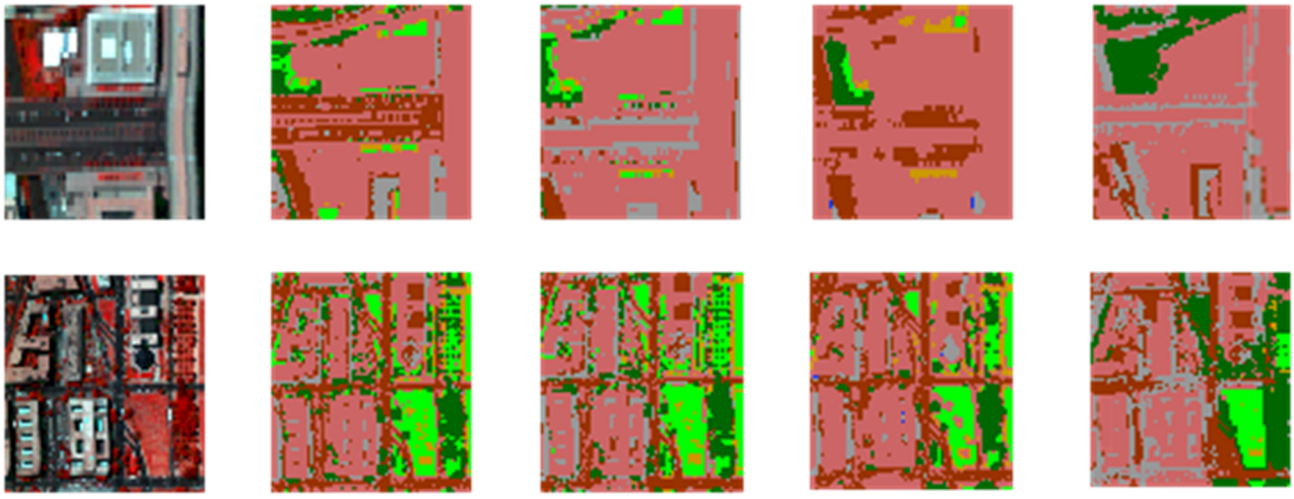

(a) original (b) Ms-SSSK (c) Ss-SSSK (d) O-SSSK (e) MSSK

Figure 13. Local image comparison.

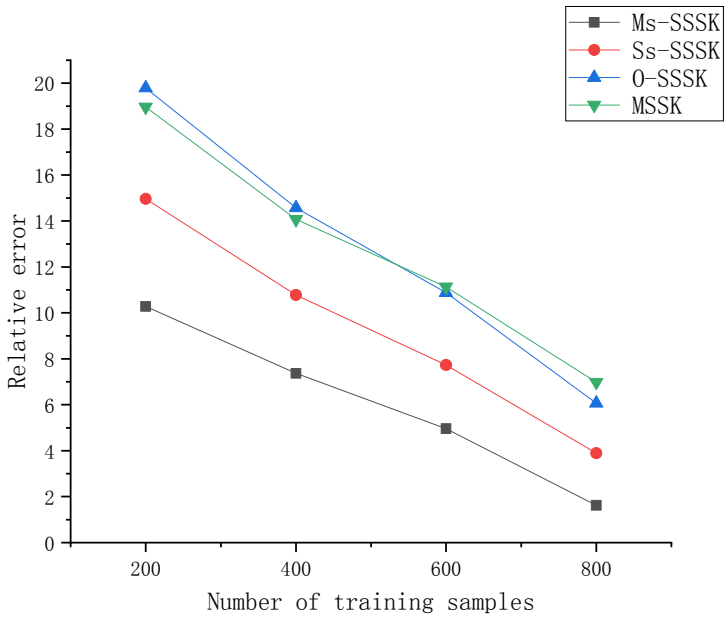

Figure 14. Relative error results of each model.

5. Conclusions

In this study, based on the high-dimensional spectral feature information of hyperspectral images, an Ms-SSSK classification model coupling multiscale superpixel spatial-spectral features and original spectral features was proposed, and hyperspectral images of the National Mall, Botswana and Pavia Centre were used as experimental objects for land use classification to comprehensively evaluate the performance of the model. The classification results were compared with the Ss-SSSK, O-SSSK and MSSK methods, from the experimental results, the following conclusions can be drawn:

1) The classification accuracy of the National Mall in Washington DC test set obtained by the Ms-SSSK method was 98.53%, which was a maximum increase of 7.56% compared to the the other three methods. The classification results of the test set showed that the model can obtain good classification accuracy in the three data sets. In addition, the classification results of the National Mall in Washington DC original images showed that Ms-SSSK more easily distinguished between woodland and grass and other spatially adjacent land types with similar spectral characteristics, and the classification effect was significantly better than those of the Ss-SSSK, O-SSSK and MSSK methods.

2) The selection of the weight μ in the Ms-SSSK method has a certain impact on the classification accuracy. When μ as 0.6, the classification accuracy was 98.53%, which was a high classification accuracy.

3) When the sample set size was 200, the classification accuracy of the Ms-SSSK model was at most 9.51 percentage points higher than that of the other three methods, which proves that the Ms-SSSK model can still obtain better classification accuracy for small samples.

The Ms-SSSK method could effectively solve the problems that the image spectrum cannot be adaptive and the spectrum information is not comprehensively acquired, and could significantly improve the land use classification accuracy. Accurately grasping the information on the current status of land resource utilization is of great significance for the preparation and implementation of future land spatial planning. Due to the different texture characteristics of plots with different uses, in the follow-up research, further combination of land texture characteristics and spectral characteristics will be considered to develop a more accurate land use classification method.

Acknowledgments

Author Contributions: Conceptualization: H. W. and W. L.. Data curation: W. L.. Formal analysis: W. L. and W. H.. Methodology: H. W., W. L., J. N. and K. N.. Experiment and result analysis: H. W. and W. L.. Visualization: W. L. and W. H.. Writing-original draft: H. W. and W. L.. Writing-review and editing: H. W., J. N. and K. N.. All authors have read and agreed to the published version of the manuscript.

Funding: This research was funded by the Open Fund Project of the Key Laboratory of Urban Land Resources Monitoring and Simulation of the Ministry of Natural Resources, grant number KF-2019-04-038. National Natural Science Foundation of China, grant number 41771438. Postgraduate Education Reform and Quality Improvement Project of Henan Province, grant number HNYJS2020JD14.

Conflict of Interests

The authors declare there is no conflict of interests.

References

1. F. Yulianto, Suwarsono, U. C. Nugroho, N. P. Nugroho, W. Sunarmodo, M. R. Khomarudin, Spatial-Temporal Dynamics Land Use/Land Cover Change and Flood Hazard Mapping in the Upstream Citarum Watershed, West Java, Indonesia, *Quaestiones Geographicae,* **39** (2020), 125–146.

2. Y. Ye, Y. An, B. Chen, J. Wang, Y. Zhong, Land use classification from social media data and satellite imagery, *J. Supercomput.,* **76** (2020), 777–792.
3. A. F. H. Goetz, Three decades of hyperspectral remote sensing of the Earth: A personal view, *Remote Sens. Environ.*, **113** (2009), S5–S16.
4. L Sun, C Ma, Y Chen, Y. Zheng, H. J. Shim, Z. Wu, Low Rank Component Induced Spatial-spectral Kernel Method for Hyperspectral Image Classification, *IEEE Trans. Circuits Syst. Video Technol.*, **2019** (2019), 3005–3008.
5. L Sun, F Wu, T Zhan, W. Liu, J. Wang, B. Jeon, Weighted Nonlocal Low-Rank Tensor Decomposition Method for Sparse Unmixing of Hyperspectral Images, *IEEE J. Sel. Top. Appl. Earth Obs. Remote Sens.,* **13** (2020), 1174–1188.
6. J. Peng, L. Li, Y. Y. Tang, Maximum Likelihood Estimation-Based Joint Sparse Representation for the Classification of Hyperspectral Remote Sensing Images, *IEEE Trans. Neural Networks Learn. Syst.,* **30** (2018), 1790–1802.
7. J. C. W. Chan, D. Paelinckx, Evaluation of Random Forest and Adaboost tree-based ensemble classification and spectral band selection for ecotope mapping using airborne hyperspectral imagery, *Remote Sens. Environ.*, **112** (2008), 2999–3011.
8. P. Rao, J. Wang, Y. Wang, Extraction of information on construction land based on multi-feature decision tree classification, *Trans. Chin. Soc. Agric. Eng.*, **30** (2104), 233–240.
9. Y. Liu, L. Wang, B. Zhang, J. Men, Scene-level land use classification based on multi-features soft-probability cascading, *Trans. Chin. Soc. Agric. Eng.*, **32** (2016), 266–272.
10. K. Rangzan, M. Kabolizadeh, D. Karimi, S. Zareie, Supervised cross-fusion method: A new triplet approach to fuse thermal, radar, and optical satellite data for land use classification, *Environ. Monit. Assess.*, **191** (2019), 481.
11. S. A. Manaf, N. Mustapha, M. N. Sulaiman, N. A. Husin, M. R. A. Hamid, Artificial Neural Networks for Satellite Image Classification of Shoreline Extraction for Land and Water Classes of the North West Coast of Peninsular Malaysia, *Adv. Sci. Lett.*, **24** (2018), 1382–1387.
12. J. Fan, T. Chen, S. Lu, Unsupervised Feature Learning for Land-Use Scene Recognition, *IEEE Trans. Geosci. Remote Sens.*, **55** (2017), 2250–2261.
13. J. Men, L. Fang, Y. Liu, Y. Sun, Land Use Classification Based on Multi-structure Convolution Neural Network Features Cascading, *Int. Arch. Photogramm. Remote Sens. Spat. Inf. Sci.*, **2019** (2019), 163–167.
14. K. Bhosle, V. Musande, Evaluation of Deep Learning CNN Model for Land Use Land Cover Classification and Crop Identification Using Hyperspectral Remote Sensing Images, *J. Indian Soc. Remote Sens.*, **47** (2019), 1949–1958.
15. S. Bera, V. K. Shrivastava, Analysis of various optimizers on deep convolutional neural network model in the application of hyperspectral remote sensing image classification, *Int. J. Remote Sens.*, **41** (2020), 2664–2683.
16. W. Huang, Y. Xu, X. Hu, Z. Wei, Compressive Hyperspectral Image Reconstruction Based on Spatial–Spectral Residual Dense Network, *IEEE Geosci. Remote Sens. Lett.*, **17** (2020), 884–888.
17. P. J. Du, J. S. Xia, Z. H. Xue, K. Tan, H. J. Su, R. Bao, Review of hyperspectral remote sensing image classification, *J. Remote Sens.*, **20** (2016), 236–256.
18. J. Fan, T. Chen, S. Lu, Superpixel Guided Deep-Sparse-Representation Learning for Hyperspectral Image Classification, *IEEE Trans. Circuits Syst. Video Technol.*, **28** (2018), 3163–3173.

19. J. Li, J. M. Bioucas-Dias, A. Plaza, Semisupervised Hyperspectral Image Segmentation Using Multinomial Logistic Regression With Active Learning, *IEEE Trans. Geosci. Remote Sens.*, **48** (2010), 4085–4098.
20. P. Ghamisi, M. S. Couceiro, F. M. Martins, J. A. Benediktsson, Multilevel Image Segmentation Based on Fractional-Order Darwinian Particle Swarm Optimization, *IEEE Trans. Geosci. Remote Sens.*, **52** (2014), 2382–2394.
21. P. Y. Wang, H. Q. Zhu, N. CHEN, UMMS: Efficient Superpixel Segmentation Driven by a Mixture of Spatially Constrained Uniform Distribution, *IEICE Trans. Inf. Syst.*, **103** (2020), 181–185.
22. D. Song, X. Tan, B. Wang, L. Zhang, X. Shan, J. Cui, Integration of super-pixel segmentation and deep-learning methods for evaluating earthquake-damaged buildings using single-phase remote sensing imagery, *Int. J. Remote Sens.*, **41** (2020), 1040–1066.
23. B. Amin, M. M. Riaz, A. Ghafoor, Automatic Image Matting of Synthetic Aperture Radar Target Chips, *Radioengineering*, **29** (2020), 228–234.
24. X. Yuan, S. Guo, C. Li, B. Lu, S. Lou, Near Infrared Star Centroid Detection by Area Analysis of Multi-Scale Super Pixel Saliency Fusion Map, *Tsinghua Sci. Technol.*, **24** (2019), 291–300.
25. K. Tang, Z. Su, W. Jiang, J. Zhang, Superpixels for large dataset subspace clustering, *Neural Comput. Appl.*, **31** (2019), 8727–8736.
26. Y. J. Chen, C. Y. Ma, Edge-Modified Superpixel Based Spectral-Spatial Kernel Method for Hyperspectral Image Classification, *Acta Electron. Sin.*, **47** (2019), 73–81.
27. Z. Liu, Y. Wu, Y. Zou, Multiscale infrared superpixel-image model for small-target detection, *J. Image Graphics*, **24** (2019), 2159–2173.
28. M. S. Chaibou, P. H. Conze, K. Kalti, M. A. Mahjoub, B. Solaiman, Learning contextual superpixel similarity for consistent image segmentation, *Multimedia Tools Appl.*, **79** (2020), 2601–2627.
29. Y. Song, W. Liu, S. Zong, Y. Luo, Segmentation Algorithm for Unmanned Aerial Vehicle Imagery Based on Superpixel and Ultrametric Contour Map, *J. Comput. Aided Des. Comput. Graphics*, **31** (2019), 1294–1300.
30. X. Hou, H. Zhao, Y. Ma, Fast Image Segmentation Algorithm Based on Superpixel Multi-feature Fusion, *Acta Electron. Sin.*, **47** (2019), 2126–2133.
31. H. Liang, B. X. Yao, P. D. Chen, Superpixel segmentation method of high resolution remote sensing images based on hierarchical clustering, *J. Infrared Millimeter Waves*, **39** (2020), 263–272.
32. Z. Yang, X. D. Mu, S. Y. Wang, C. H. Ma, Scene classification of remote sensing images based on multiscale features fusion, *Opt. Precis. Eng.*, **26** (2018), 3099–3107.
33. D. Zhang, T. Yin, G. Yang, M. Xia, L. Li, X. Sun, Detecting image seam carving with low scaling ratio using multi-scale spatial and spectral entropies, *J. Visual Commun. Image Representation*, **48** (2017), 281–291.
34. Z. Chen, X. Wang, K. Yan, J. Zheng, Deep multi-scale feature fusion for pancreas segmentation from CT images, *Int. J. Comput. Assisted Radiol. Surg.*, **15** (2020), 415–423.
35. Hyperspectral Image, the National Mall in Washington DC. Available from: https://engineering.purdue.edu/~biehl/MultiSpec/hyperspectral.html.
36. M Graña, M. A Veganzons, B Ayerdi, Hyperspectral Remote Sensing Scenes. Available from: http://www.ehu.eus/ccwintco/index.php?title=Hyperspectral_Remote_Sensing_Scenes.

37. X. Jia, J. A. Richards, Segmented principal components transformation for efficient hyperspectral remote-sensing image display and classification, *IEEE Trans. Geosci. Remote Sens.*, **37** (1999), 538–542.
38. X. Kang, P. Duan, S. Li, Hyperspectral image visualization with edge-preserving filtering and principal component analysis, *Inf. Fusion*, **57** (2020), 130–143.
39. B. Fatima, A. R. Shahid, S. Ziauddin, A. A. Safi, H. Ramzan, Driver Fatigue Detection Using Viola Jones and Principal Component Analysis, *Appl. Artif. Intell.*, **34** (2020), 456–483.
40. Z. Zhang, J. Liu, Z. Xi, A disparity optimization algorithm using entropy rate super-pixel segmentation consistency check, *Comput. Eng. Appl.*, **56** (2020), 1–8.
41. Liu Xia, Guo Yanan, Remote sensing image change detection algorithm based on random forest, *Bull. Surv. Mapp.*, **5** (2020), 16–20.
42. C. Shi, C. M. Pun, Multiscale Superpixel-Based Hyperspectral Image Classification Using Recurrent Neural Networks With Stacked Autoencoders, *IEEE Trans. Multimedia*, **22** (2020), 487–501.
43. C. G. Karydas, Optimization of multi-scale segmentation of satellite imagery using fractal geometry, *Int. J. Remote Sens.*, **41** (2020), 2905–2933.
44. L Sun, C Ma, Y Chen, H. J. Shim, Z. Wu, B. Jeon, Adjacent superpixel-based multiscale spatial-spectral kernel for hyperspectral classification, *IEEE J. Selected Topics in Applied Earth Observations Remote Sens.*, **12** (2019), 1905–1919.
45. C. Liu, L. Hong, J. Chen, S. S. Chun, M. Deng, Fusion of pixel-based and multi-scale region-based features for the classification of high-resolution remote sensing image, *J. Remote Sens.*, **19** (2015), 228–239.
46. G. Camps-Valls, L. Bruzzone, Kernel-based methods for hyperspectral image classification, *IEEE Trans. Geosci. Remote Sens.*, **43** (2005), 1351–1362.
47. Y. Chen, J. Wang, R. Xia, Q. Zhang, Z. Cao, K. Yang, The Visual Object Tracking Algorithm Research Based on Adaptive Combination Kernel, *J. Ambient Intell. Humanized Comput.*, **10** (2019), 4855–4867.
48. Y. Chen, J. Xiong, W. Xu, J. Zuo, A novel online incremental and decremental learning algorithm based on variable support vector machine, *Cluster Comput.*, **22** (2019), 7435–7445.
49. Y. Chen, W. Xu, J. Zuo, K. Yang, The fire recognition algorithm using dynamic feature fusion and IV-SVM classifier, *Cluster Comput.*, **22** (2019), 7665–7675.
50. K. Shankar, S. K. Lakshmanaprabu, D. Gupta, A. Maseleno, V. Hugo, C. de Albuquerque, Optimal feature-based multi-kernel SVM approach for thyroid disease classification, *J. Supercomput.*, **76** (2020), 1128–1143.
51. M. Ramzan, A. Abid, H. U. Khan, S. M. Awan, A. Ismail, M. Ahmed, et al., A Review on State-of-the-Art Violence Detection Techniques, *IEEE Access*, **7** (2019), 107560–107575.
52. C. C. Chang, H. T. Huang, Automatic Tuning of the RBF Kernel Parameter for Batch-Mode Active Learning Algorithms: A Scalable Framework, *IEEE Trans. Cybern.*, **49** (2019), 4460–4472.
53. K. Shang, P. Li, T. Cheng, Land Cover Classification of Hyperspectral Data Using Composite Kernel Support Vector Machines, *Acta Sci. Nat. Univ. Pekin.*, **7** (2019), 107560–107575.

AIMS Press